THE JOURNAL OF PHYSICAL CHEMISTRY B

Article

pubs.acs.org/JPCB

On the Shape of the Phonon Spectral Density in Photosynthetic Complexes

Adam Kell,[†] Ximao Feng,[†] Mike Reppert,[§] and Ryszard Jankowiak*[,†,‡,∥,⊥]

[†]Department of Chemistry and [‡]Department of Physics, Kansas State University, Manhattan, Kansas 66506, United States

[§]Department of Chemistry, Massachusetts Institute of Technology, Cambridge, Massachusetts 02139, United States

[∥]Faculty of Applied Physics and Mathematics, Gdańsk University of Technology, 80-233 Gdańsk, Poland

Supporting Information

ABSTRACT: We provide a critical assessment of typical phonon spectral densities, $J(\omega)$, used to describe linear and nonlinear optical spectra in photosynthetic complexes. Evaluation is based on a more careful comparison to experiment than has been provided in the past. $J(\omega)$ describes the frequency-dependent coupling of the system to the bath and is an important component in calculations of excitation energy transfer times. On the basis of the shape of experimental $J(\omega)$ obtained for several photosynthetic complexes, we argue that the shape of $J(\omega)$ strongly depends on the pigment−protein complex. We show that many densities (especially the Drude−Lorentz/constant damping Brownian oscillator) display qualitatively wrong behavior when compared to experiment. Because of divergence of $J(\omega)$ at zero frequency, the Brownian oscillator cannot fit a single-site spectrum correctly. It is proposed that a log-normal distribution can be used to fit experimental data and exhibits desired attributes for a physically meaningful phonon $J(\omega)$, in contrast to several commonly used spectral densities which exhibit low-frequency behavior in qualitative disagreement with experiment. We anticipate that the log-normal $J(\omega)$ function proposed in this work will be further tested in theoretical modeling of both time- and frequency-domain data.

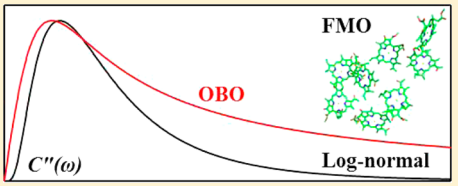

1. INTRODUCTION

The primary input into energy transfer and line shape calculations for excitonic systems is a spectral density, $J(\omega)$, which describes the coupling of the electronic transition to matrix vibrations. Rate constants for exciton transfer, as well as line shape functions of optical transitions, strongly depend on the shape of $J(\omega)$ of exciton-vibration coupling.[1] Although experimental data clearly indicate that the shape of $J(\omega)$ varies depending on the photosynthetic system under consideration,[2−4] in theoretical studies standard functional forms are often assumed for $J(\omega)$ which either deviate significantly from experimental data or are valid only for specific systems.[5] Many efforts have been undertaken to extract the bath spectral densities from mixed quantum-classical calculations.[6−9] Various semiclassical corrections to the spectral density have also been investigated.[9] Direct calibration against experiment, however, is generally difficult due to the inherently broad spectral transitions observed for room temperature photosynthetic complexes.

Below, we provide a critical assessment of $J(\omega)$ typically used to describe linear and nonlinear optical spectra, such as those obtained from spectral hole-burning (SHB) and two-dimensional electronic spectroscopy (2DES). We argue that many functions used so far either poorly describe the shape of $J(\omega)$ or cause clear difficulties in spectral calculations.

To avoid confusion, we adopt the definition of May and Kühn for $J(\omega)$:[10]

$$J(\omega) = \sum_i s_i \delta(\omega - \omega_i) \tag{1}$$

with $s_i = \omega_i d_i^2/2\hbar$, the dimensionless Huang−Rhys factor for each bath mode indicating the strength of electron−phonon coupling. Here, ω_i is the frequency of the ith bath mode and d_i is the displacement of the ith bath mode minimum in the ground and excited electronic state potential energy surfaces. $J(\omega)$ (in units of angular frequency) is sometimes referred to as the phonon profile and defines the total Huang−Rhys factor[10]

$$S = \int_0^\infty J(\omega)\, \mathrm{d}\omega = \sum_i s_i \tag{2}$$

and reorganization energy

$$E_\lambda = \hbar \int_0^\infty \omega J(\omega)\, \mathrm{d}\omega \tag{3}$$

Under this definition, $J(\omega)$ differs by a factor of ω^2 from the antisymmetric component of the Fourier−Laplace transform of the energy gap correlation function

$$C''(\omega) = \omega^2 J(\omega) \tag{4}$$

which is itself sometimes referred to as the spectral density.[11] As the primary determinant of system−bath interactions in model calculations for excitonically coupled systems, $J(\omega)$

Received: May 23, 2013
Revised: May 29, 2013
Published: May 29, 2013

directly determines both spectral characteristics and exciton relaxation dynamics.[12]

Although $J(\omega)$ can be obtained by delta fluorescence line-narrowing (ΔFLN) spectroscopy,[2−4] to be useful one needs to express its shape by a function that can be used in theoretical calculations of the line shape functions and excitation energy transfer (EET) rates. The shape of the spectral density is critical to properly describe various optical spectra and, in particular, exciton relaxation processes. Specifically, we suggest that for photosynthetic systems a proper model for $J(\omega)$ should (1) converge to zero as frequency approaches zero, (2) ensure that the quantity $\omega^2 J(\omega)$ converges to zero at infinite frequency, and (3) fit the experimental profile obtained for $J(\omega)$. The first condition has already been briefly discussed by Toutounji and Small[12] in the context of zero-phonon line (ZPL) widths and is necessary to ensure that the phonon sideband in optical spectra decays toward zero near the ZPL, as consistently observed in experimental data. Note also that without this condition the Huang−Rhys factor may be undefined. The second criterion provides a well-defined value for E_λ and ensures under certain conditions (e.g., Redfield relaxation) that the energy transfer rate decays to zero at infinite energetic separation. For simple line shape and dynamics calculations (e.g., Förster or Redfield relaxation rates) these three conditions suffice, as all required spectral manipulations can be performed numerically. However, for more advanced calculations a convenient analytical form of the function may also be important. This is one of the reasons why many theoretical papers use either an Ohmic density with exponential cutoff or the overdamped Brownian oscillator (OBO) (*vide infra*). The functions describing $J(\omega)$, along with corresponding equations defining S and E_λ, are summarized in the Supporting Information.

In the case where molecules are coupled to a continuum of low-frequency, damping modes and a single high-frequency mode, the antisymmetric component can be written as[13]

$$C''(\omega) = C_0''(\omega) + C_{\mathrm{vib}}''(\omega) \tag{5}$$

Of course, coupling to multiples modes, especially on the low-frequency part of the vibronic spectrum (up to ∼500 cm^{-1}), might be relevant for energy transfer in the Fenna−Matthews−Olson (FMO) complex.[14] In eq 5, the (fast) $C_0''(\omega)$ mode corresponds to the a smooth background describing fluctuations due to the protein environment, while the second term expresses couplings to one or multiple discrete vibrational modes, which may be of intramolecular origin. Thus, the second term, $C_{\mathrm{vib}}''(\omega)$, represents the spectral density of (slow) molecular vibrations (*damped* or *undamped*) whose importance was recently addressed in the context of molecular vibrations in 2DES signals.[13] The influence of fast vibrations on energy transfer continues to be of great interest; for example, recently Kolli et al.[15] showed the importance of high-energy quantized vibrations and their nonequilibrium dynamics for energy transfer in photosynthetic systems with highly localized excitonic states. Finally, we note that vibrational frequencies and their Huang−Rhys factors can be measured by ΔFLN[16] and hole-burning (HB) spectroscopies.[17] In this article, however, we focus only on the phonon spectral density.

2. RESULTS AND DISCUSSION

Below we provide careful comparison of various spectral densities to experimental data. For example, we show that divergence of $J(\omega)$ at zero frequency is in qualitative disagreement with experimental data. We argue that the OBO and Ohmic densities (*vide infra*) cannot fit a single-site spectrum correctly. We begin with a brief description and comparison of phonon spectral densities used so far in modeling studies. We focus on shortcomings and advantages of various functions used in theoretical calculations of optical spectra and EET rates in photosynthetic complexes.

2.1. Gaussian−Lorentzian (G−L). The empirical function given by a Gaussian distribution on the low-energy side and a Lorentzian distribution on the high-energy side (see Supporting Information) is often used in modeling of HB spectra and experimental $J(\omega)$ obtained by ΔFLN spectra[2−4] because its asymmetric shape is similar to experiment. Also, specific line shape characteristics, peak position and full width at half-maximum, are input parameters—making adjustments to the line shape simple and intuitive. This function, however, leads to infinitely large E_λ (*vide infra*) and cannot be used in energy transfer rate expressions. Problems can also arise in calculations of the ZPL, as certain values for peak position and Gaussian width result in a $J(\omega)$ that does not decay to zero at zero frequency, leading to an unphysical broadening of the ZPL.[12]

2.2. B777. The B777 spectral density,[5] used in Redfield-based calculations of optical spectra of photosynthetic complexes and given below (eq 6), was obtained from the 1.6 K FLN spectra measured for B777 complexes from LH1. The B777 complex contains a single bacteriochlorophyll *a* molecule bound to a single α-helix protein.[5]

$$J(\omega) = \frac{S_0}{s_1 + s_2} \sum_{i=1,2} \frac{s_i}{7!2\omega_i^4} \omega^3 \mathrm{e}^{-(\omega/\omega_i)^{1/2}} \tag{6}$$

where $s_1 = 0.8$, $s_2 = 0.5$, $\hbar\omega_1 = 0.069$ meV (0.56 cm^{-1}), and $\hbar\omega_2 = 0.24$ meV (1.9 cm^{-1}). $J(\omega)$ given by eq 6 is qualitatively reasonable (i.e., it captures the right physical trend; *vide infra*), but its shape could be improved by comparing to the shape of experimental ΔFLN spectra. Concerning the exciton-vibration coupling, ΔFLN spectra (not FLN spectra) provide valuable information on the spectral density; i.e., FLN signals and ΔFLN signals collected under the same conditions are not proportional to each other.[16,18] Only ΔFLN spectra reduce directly to the single-site fluorescence line shape function in the low-fluence limit,[16] providing information on the phonon spectral density. While the B777 $J(\omega)$ has been applied to various photosynthetic complexes,[19−22] due to the simplistic nature of the B777 protein it cannot represent a generic spectral density observed experimentally in various photosynthetic complexes, e.g., FMO,[2] the minor light harvesting antenna (CP29) from photosystem II (PSII),[3] the water-soluble chlorophyll binding protein (WSCP).[4] This is especially true for the shape of $J(\omega)$ for WSCP (*vide infra*), which has three clearly distinguishable peaks.[4] It has also been noted before that there exist differences between the B777 density and the G−L $J(\omega)$[23] of the major light harvesting complex in PSII (LHCII), although it was suggested that the differences could be due to low-frequency protein vibrations improperly assigned as intramolecular modes.[22]

Approximate functions have been proposed in the literature for the B777 $C''(\omega)$ when applied to the B850 band of the LH2 antenna of purple bacteria,[24−27] where application of the B777 $J(\omega)$ would be most warranted due to the similar pigment−protein interactions (i.e., LH1 and LH2 have similar pigment−protein subunits[5]). The alternative functions were used to preserve the peak position and shape of $C''(\omega)$ and to simplify calculations with the use of an interpolated formula when

dx.doi.org/10.1021/jp405094p | J. Phys. Chem. B 2013, 117, 7317−7323

calculating the correlation function.[25,28] These approximations were sums of Ohmic-like densities discussed below. A three-term super-Ohmic density was also used to approximate the B777 function when applied to bacterial reaction centers with charge transfer states.[29]

2.3. Brownian Oscillator. An often-used functional form for the spectral density is the OBO or Drude−Lorentz density, which depends on E_λ, and a damping constant, γ:[11]

$$C''(\omega) = \frac{2E_\lambda \gamma \omega}{\hbar\pi(\omega^2 + \gamma^2)} \tag{7}$$

Often when this function is used for $C''(\omega)$, π^{-1} is included as part of E_λ. To keep our definitions consistent throughout the text, the π term is included in the denominator of the OBO function. This overdamped function is a special case of the more general multimode BO (MBO) density obtained by assuming constant damping for a single mode at zero frequency.[11] Constant damping implies that

$$J(\omega) \sim \frac{1}{\omega} \quad \text{as } \omega \to 0 \tag{8}$$

Under this assumption the OBO $J(\omega)$ mentioned above diverges at zero frequency, meaning that the Huang−Rhys factor is undefined and, as a result, the OBO $J(\omega)$ will never fit single-site spectra correctly. Aside from failing to accurately describe experimental SHB line shapes, this leads to the intuitively undesirable result that single-site absorption and emission spectra can no longer be divided cleanly into R-phonon excitation profiles.[17] The careful modeling of the continuous part of the spectral density toward zero frequency is essential for the prevalence of coherence in molecular networks because it determines the pure dephasing rate, γ_d.[30] Also, the OBO $J(\omega)$ does not yield long lasting cross-peak oscillations in 2D echo spectra of the seven-site FMO complex.[30−32]

The more general MBO model is often used for describing high-frequency vibrations,[6,33] while a modified OBO, the quantum overdamped bath function, has been proposed as it overcomes the slow Lorentzian decay of the standard OBO.[13] However, if constant damping is assumed, both the MBO and quantum OBO functions suffer from the same drawbacks encountered by the standard overdamped form (e.g., infinite value at zero frequency and undefined S).

2.4. Ohmic. Another common function is the Ohmic-type spectral density of the form[10]

$$C''(\omega) = \eta\omega\left(\frac{\omega}{\omega_c}\right)^{\alpha-1} e^{-\omega/\omega_c} \tag{9}$$

where α is the order of the function and η is a normalization factor that is directly proportional to E_λ (see Supporting Information for details). The B777 function described earlier (see eq 6) is a sum of several densities with closely related forms (although the exponential cutoff in B777 is raised to the power of 1/2). Three types of densities can be distinguished: (i) sub-Ohmic ($0 < \alpha < 1$), (ii) Ohmic ($\alpha = 1$), and (iii) super-Ohmic ($\alpha > 1$)—all of which are simply Gamma distributions multiplied by ω with various shape parameters (divided by ω^2 in the case of $J(\omega)$). Note that the designation of a density as "Ohmic" reflects the behavior of $C''(\omega)$ at zero frequency: any Ohmic or sub-Ohmic choice for $C''(\omega)$ will result in a $J(\omega)$ that diverges at zero frequency, which is in qualitative disagreement with experiment.[2−4]

2.5. Log-Normal. On the basis of our extensive search for functions that could describe experimental $J(\omega)$ in several photosynthetic complexes, we found that the log-normal distribution defined below is an excellent choice:

$$J(\omega) = \frac{S}{\sigma\omega\sqrt{2\pi}} e^{-[\ln(\omega/\omega_c)]^2/2\sigma^2} \tag{10}$$

where ω_c is the cutoff frequency and σ is the standard deviation. This line shape is advantageous because it converges for large frequencies (e.g., both S and E_λ are defined) and has an adjustable asymmetry which describes very well the experimental $J(\omega)$ and various optical spectra (to be reported elsewhere). This function also contains two adjustable parameters (ω_c and σ), unlike the other functions discussed previously, which rely solely on a cutoff frequency or damping constant (with the exception of G-L) as S and E_λ only affect normalization/peak amplitude. See Table S1 in the Supporting Information for how parameters affect the shapes of different spectral densities.

2.6. Application to Photosynthetic Antenna Complexes. In this section, we present comparisons of a number of spectral density models with experimental data for a variety of photosynthetic complexes. Figures 1 and 2 focus on the FMO

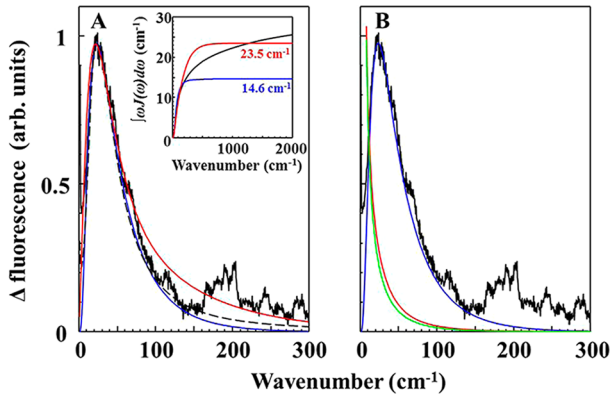

Figure 1. Frame A: experimental FMO (*tepidum*) ΔFLN spectrum (black, ω_{ex} = 12 090 cm^{-1})[2] and single-site spectra calculated with G-L (black dashed, ω_m = 22 cm^{-1}, Γ_G = 22 cm^{-1}, Γ_L = 60 cm^{-1}),[2] log-normal (blue, ω_c = 38 cm^{-1}, σ = 0.7) and B777 (red) functions. The inset shows the integral of $\omega J(\omega)$ (S = 0.3) for the corresponding curves. Frame B: ΔFLN and log-normal curves from frame A with single-site spectra calculated with OBO (red, γ = 53 cm^{-1}) and Ohmic (ω_c = 50 cm^{-1}) functions. OBO and Ohmic fits scaled to match fwhm of ZPL (not shown).

antenna complex. The FMO complex is an often-studied system due to the presence of long-lasting quantum coherence exhibited in 2D spectra,[34,35] and all functions mentioned in this text have been applied to model exciton relaxation and optical spectra of FMO. Figure 1 shows calculated single-site spectra compared to the experimental ΔFLN spectrum for FMO (*Chlorobaculum tepidum*),[2] as the shape of the phonon spectral density directly determines the phonon sideband of the single-site spectrum.[17] Using the often-published parameter values for the B777 density leads to a broadened single-site spectrum that cannot fit the experimental data (frame A). It should be noted that the main argument for using the B777 function to describe FMO comes from Figure 2 of ref 19. There, $J(\omega)$ is compared directly to the experimental 4 K FLN spectrum (not ΔFLN as shown in this work) of FMO (*Prosthecochloris aestuarii*). For

dx.doi.org/10.1021/jp405094p | J. Phys. Chem. B 2013, 117, 7317−7323

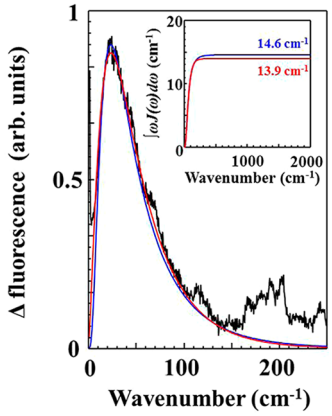

Figure 2. Experimental FMO (*tepidum*) ΔFLN spectrum (black, ω_{ex} = 12 090 cm^{-1})[2] and single-site spectra calculated with log-normal (blue, ω_c = 38 cm^{-1}, σ = 0.7) and modified B777 (red, s_1 = 1, s_2 = 0, $\hbar\omega_1$ = 0.08 meV = 0.65 cm^{-1}, $\hbar\omega_2$ = 0) functions. The inset shows the integral of $\omega J(\omega)$ (S = 0.3) for each curve.

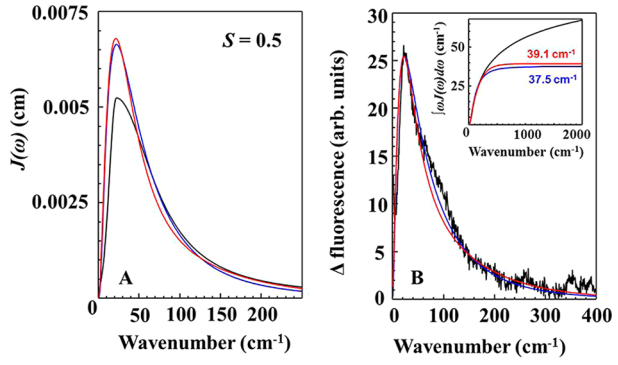

Figure 3. Frame A: $J(\omega)$ curves obtained using the G−L (black, ω_m = 22 cm^{-1}, Γ_G = 20 cm^{-1}, Γ_L = 110 cm^{-1}),[3] log-normal (blue, ω_c = 50 cm^{-1}, σ = 0.9) and B777 (red) functions for CP29. Frame B: experimental CP29 ΔFLN spectrum (black, ω_{ex} = 14 620 cm^{-1})[3] and single-site spectra calculated with log-normal (blue) and B777 (red) $J(\omega)$ from frame A. The inset shows the integral of $\omega J(\omega)$ (S = 0.5) for the corresponding curves.

comparison, frame B plots the same experimental absorption spectrum together with the diverging $J(\omega)$ profiles for the OBO and Ohmic functions. Although viable single-site absorption spectra can be calculated from these functions, due to the divergence of $J(\omega)$ at zero frequency the corresponding spectra do not display a well-defined phonon sideband; giving rise instead to broadening of the ZPL.[12]

The B777 density with modified parameters can be used to fit the *tepidum* data using only one term (i.e., s_2 = 0), as seen in Figure 2. Doing so, however, limits the function to one adjustable parameter, ω_1, which will change both the peak position and curve width simultaneously. A theoretical spectral density for FMO could be directly obtained using a normal-mode analysis,[36] though the average diagonal part of such a spectral density obtained for the monomeric subunit of the FMO protein significantly differed from the experimental average phonon spectral density obtained in ref 19 (eq 6 with S_0 = 0.5). The authors argued the deviation was likely due to anharmonicities experienced by the soft degrees of freedom that govern the conformational flexibility of the macromolecule.[1] Other studies have been made to directly determine, and fit with an analytical form, the energy gap autocorrelation function using molecular dynamics and electronic structure calculations.[6,8,9]

The CP29 antenna complex is involved in energy transfer within PSII. Frame A of Figure 3 shows the log-normal distribution (ω_c = 50 cm^{-1}, σ = 0.9)[37] compared to the published G−L (ω_m = 22 cm^{-1}, Γ_G = 20 cm^{-1}, Γ_L = 110 cm^{-1})[3] and B777 densities. The G−L from ref 3 has a different line shape compared to the others due to an improper contribution attributed to the pseudophonon sideband in the ΔFLN data; however, this function cannot be used in calculations due to the lack of a well-defined E_λ (see inset of frame B). Using a log-normal fit to the G−L parameters above, as opposed to fitting ΔFLN data, for simultaneous calculations of various optical spectra results in site energies that are ∼30 cm^{-1} higher than those published recently[37] (data not shown). Thus, the precise shape of the spectral density is needed to obtain reliable site energies from modeling studies. The log-normal and B777 calculated single-site spectra compared to the experimental data are shown in frame B of Figure 3. For CP29, both the log-normal and B777 functions fit the experimental data very well.

A small pigment−protein complex that is neither bound to the thylakoid membrane nor directly involved in photosynthesis, WSCP of higher plants is a tetramer binding Chl *a* or Chl *b*.[38] ΔFLN data for WSCP from cauliflower have shown that $J(\omega)$ has three distinct bands that contribute to the phonon sideband, which are suggested to arise from delocalized vibrations that correspond to the protein tetramer, dimer, and monomer.[4] Figure 4 shows the fit of the single-site spectrum

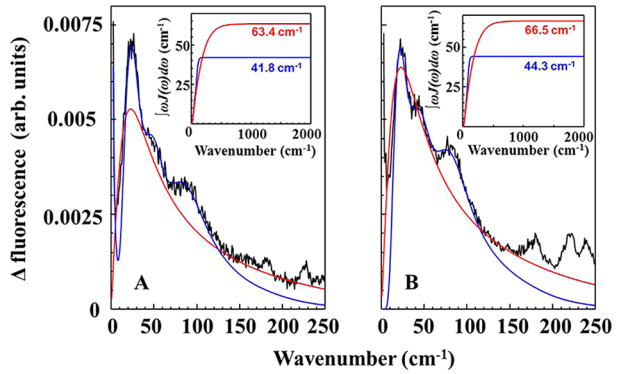

Figure 4. Frame A: experimental Chl *a*-WSCP (cauliflower) ΔFLN spectrum (black, ω_{ex} = 14 596 cm^{-1})[4] and single-site spectra calculated with log-normal (blue) and B777 (red) functions. Frame B: experimental Chl *b*-WSCP (cauliflower) ΔFLN spectrum (black, ω_{ex} = 15 006 cm^{-1})[4] and single-site spectra calculated with log-normal (blue) and B777 (red) functions. For the three term log-normal curves, parameters are listed in Table 1. Inset of each frame shows the integral of $\omega J(\omega)$ (S = 0.81 and 0.85 for Chl *a* and Chl *b*, respectively) for the corresponding curves.

calculated using the log-normal distribution with the experimental ΔFLN data for WSCP from cauliflower. To account for the detail available for WSCP, the log-normal $J(\omega)$ used is a sum of three functions with parameters reported in Table 1. Also shown in Figure 4 is the published B777 function, which has been applied to WSCP in calculations of optical spectra.[20,39] The B777 density is qualitatively similar to the ΔFLN signal in peak position and width; however, it cannot reproduce the multiple peaks seen in experiment, meaning it will underestimate the contribution from phonon modes at certain peak positions (i.e., 24 and 88 cm^{-1} for Chl *a* and 82

dx.doi.org/10.1021/jp405094p | J. Phys. Chem. B 2013, 117, 7317−7323

Table 1. Log-Normal Distribution Parameters Used To Fit ΔFLN Spectra for Chl *a*- and Chl *b*-WSCP from Cauliflower[a]

Chl *a*	ω_c (cm^{-1})	σ	S_i	Chl *b*	ω_c (cm^{-1})	σ	S_i
1	28	0.4	0.45	1	26	0.4	0.39
2	54	0.2	0.15	2	51	0.25	0.23
3	90	0.2	0.21	3	85	0.2	0.23

[a] S_i is the relative contribution of each term to the total integrated area, which is 0.81 and 0.85 for Chl *a* and Chl *b*, respectively.[4]

cm^{-1} for Chl *b*). The B777 parameters also overestimate the reorganization energy by ∼20 cm^{-1}, as seen in the insets of Figure 4.

A comparison of Ohmic-type curves with the experimentally determined log-normal $J(\omega)$ for FMO is shown in Figure 5.

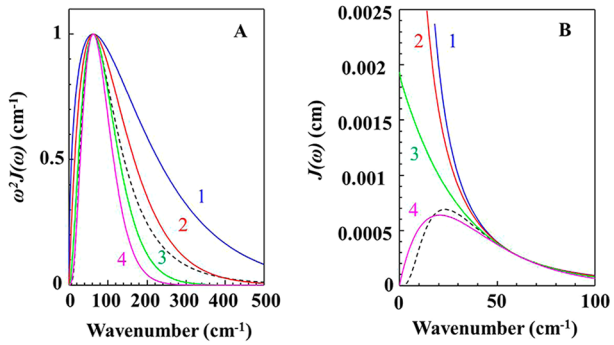

Figure 5. Frame A: curves 1−4 are normalized Ohmic-type functions (eq 9) obtained for the following parameters: (1) α = 0.5, ω_c = 124 cm^{-1}; (2) α = 1, ω_c = 62 cm^{-1}; (3) α = 2, ω_c = 31 cm^{-1}; (4) α = 3, ω_c = 20.7 cm^{-1}. The dashed curve is the FMO log-normal $J(\omega)$, multiplied by ω^2. Frame B: corresponding $J(\omega)$, i.e., the curves in frame A divided by ω^2.

Curves 1−4 are obtained from eq 9 with α = 0.5, 1, 2, and 3, respectively, while the dashed curve is the log-normal $J(\omega)$ used to calculate the single-site spectrum in Figure 1. Frames A and B show $\omega^2 J(\omega)$ and $J(\omega)$ for the parameters above, respectively. In frame A, all curves are normalized to the peak position, and it is clear that the discrepancies between different Ohmic curves are greater on the high-frequency side of the peak position. However, all curves in frame A display the same qualitative shape. When one compares the corresponding $J(\omega)$ curves (frame B), it becomes evident that only super-Ohmic (α > 3) curves display the same qualitative shape as $J(\omega)$ derived from ΔFLN data. Even though the super-Ohmic (α = 2) curve converges at zero frequency (S has a finite value), the curve poorly describes the experimental $J(\omega)$ and $\omega^2 J(\omega)$ curves. The nonzero phonon contribution at zero frequency will also introduce broadening effects to the ZPL.[12]

A comparison of both Ohmic (α = 1) and OBO curves, using parameters published previously for FMO, to the log-normal curve is shown in Figure 6. The ω_c values for the Ohmic curves are 50,[40] 100,[41] and 150 cm^{-1} [42] for curves 1−3, respectively (frame A). The γ values for the OBO curves are 32,[43] 53[44] and 106 cm^{-1} [45] (which correspond to γ^{-1} values of 166, 100, and 50 fs), respectively (frame B). Note that Ohmic and OBO curves with ω_c and γ ∼ 50 cm^{-1} match the peak position of the log-normal curve fairly well (see also curve 2 in frame A of Figure 5). However, the corresponding $J(\omega)$ functions diverge at zero frequency and S is undefined, as seen in Figure 5 for the

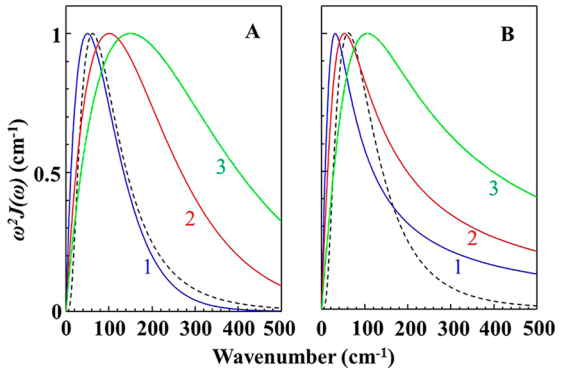

Figure 6. Frame A: normalized curves for the Ohmic (α = 1) function. Curves 1−3 were obtained with ω_c values of 50, 100, and 150 cm^{-1}, respectively (see eq 8). Frame B: normalized curves defined by eq 7 for the OBO function. Curves 1−3 were obtained with γ values of 32, 53, and 106 cm^{-1} (which correspond to γ^{-1} values of 166, 100, and 50 fs), respectively. In each frame, the dashed curve is the FMO log-normal $J(\omega)$, multiplied by ω^2.

Ohmic function. For both the Ohmic and OBO functions, the peak position and width are dependent upon the same parameter (ω_c and γ, respectively), i.e., as the peak position increases in frequency the curve broadens. Thus, if the peak position is not matched, then the resulting curves are too broad and high-frequency modes are improperly weighted. This is truer of the OBO function than of the Ohmic due to the OBO function having a slow Lorentzian decay.

3. CONCLUDING REMARKS

We have demonstrated that many shapes of the commonly used spectral densities, especially the OBO (or Drude−Lorentz) and Ohmic $J(\omega)$, are qualitatively wrong in comparison to experiment. The B777 $J(\omega)$ (with a qualitatively reasonable shape) can only be used if its parameters can be adjusted to fit experimental ΔFLN spectra. We have shown that experimentally measured $J(\omega)$ of FMO, the CP29 antenna complex of PSII and WSCP can be well described using the proposed log-normal function. On the basis of the examples discussed above, it is clear that the shape of $J(\omega)$ strongly depends on the pigment−protein complex. This is not surprising, as the interaction of the vibrations with different environments will vary from system to system (it is the protein environment that adjusts the pigment site energies). Pigment binding to the protein scaffolding may also affect frequency and intensity of existing chromophore vibrations. This could lead to frequency shifts or suppression of certain backbone motions by formation of additional bonds to the protein environment; the latter was illustrated by ΔFLN spectra obtained recently for WSCP.[4] Thus, the functional form of $J(\omega)$ is very important for further refinement of various theoretical models describing the spectral line shape and, in particular, population dynamics in photosynthetic complexes.[8,14,19,40] We suggest that the G−L $J(\omega)$ used in modeling of HB spectra should be replaced with the log-normal function or B777 (with adjusted parameters), which provides a more physically realistic fit of the high-energy side of experimental spectral densities. The absence of the long Lorentzian tail in the log-normal function eliminates problems associated with continuously increasing E_λ, which is not well-defined since the integral does not converge for the Lorentzian. The log-normal form also solves problems with the zero frequency behavior of the constant damping BO $J(\omega)$, which

dx.doi.org/10.1021/jp405094p | J. Phys. Chem. B 2013, 117, 7317−7323

contradicts experiment. We anticipate that the $J(\omega)$ function proposed in this work (see eq 10) will be successfully tested in theoretical modeling of both time- and frequency-domain data.

Despite the central role that the spectral density plays in excitonic dynamics and energy relaxation, a thorough general understanding of how specific spectral density features influence dynamics is still lacking. Here we only note that very recently it has been demonstrated that electronic coherence and fast thermalization depend sensitively on the continuum part of the spectral density;[30] therefore, it is critical to use functions that properly describe the experimental $J(\omega)$. In modeling of 2DES data obtained for photosynthetic complexes, both parts of the antisymmetric component, i.e., $C_0''(\omega)$ and $C_{vib}''(\omega)$, need to be considered,[13] as coherent excitonic dynamics may assist coupling to selected modes that channel energy to preferential sites in the complex.[15] The effect of various spectral densities on the calculated 2DES spectra, in particular on the extent of long-lasting and purely electronic, electronic/vibronic, or vibronic coherence, has been discussed in ref 13. Thus, we conclude that experimentally determined $J(\omega)$ must be used in modeling studies of a particular protein complex, as its shape is very important in the proper description of bath relaxation dynamics associated with the exciton transfer process. For example, careful modeling of the continuous part of the $J(\omega)$ toward zero frequency is essential for the prevalence of coherence in molecular networks because it determines the pure dephasing rate.[30]

■ ASSOCIATED CONTENT

Supporting Information

Basic definitions, relevant equations, and parameter descriptions for often used spectral densities. This material is available free of charge via the Internet at http://pubs.acs.org.

■ AUTHOR INFORMATION

Corresponding Author

*E-mail ryszard@ksu.edu (R.J.).

Notes

The authors declare no competing financial interests.

[⊥]R.J.: On a sabbatical leave from Kansas State University, Manhattan, KS 66506.

■ ACKNOWLEDGMENTS

This work was supported by the Chemical Sciences, Geosciences and Biosciences Division, Office of Basic Energy Sciences, Office of Science, U.S. Department of Energy (Grant DE-FG02-11ER16281 to R.J.). Partial support for A.K. was provided by European Social Fund's Doctoral Studies and Internationalisation Programme DoRa during a short research visit to the University of Tartu (UT), Tartu, Estonia. We acknowledge useful discussions with Jörg Pieper(UT) and Arvi Freiberg (UT) and Margus Rätsep (UT) and Jörg Pieper for sharing with us $x-y$ data of their previously published ΔFLN spectra.

■ REFERENCES

(1) Renger, T.; Müh, F. Understanding Photosynthetic Light-Harvesting: A Bottom Up Theoretical Approach. *Phys. Chem. Chem. Phys.* **2013**, *15*, 3348−3371.

(2) Rätsep, M.; Freiberg, A. Electron-Phonon and Vibronic Couplings in the FMO Bacteriochlorophyll *a* Antenna Complex Studied by Difference Fluorescence Line Narrowing. *J. Lumin.* **2007**, *127*, 251−259.

(3) Rätsep, M.; Pieper, J.; Irrgang, K.-D.; Freiberg, A. Excitation Wavelength-Dependent Electron-Phonon and Electron-Vibrational Coupling in the CP29 Antenna Complex of Green Plants. *J. Phys. Chem. B* **2008**, *112*, 110−118.

(4) Pieper, J.; Rätsep, M.; Trostmann, I.; Paulsen, H.; Renger, G.; Freiberg, A. Excitonic Energy Level Structure and Pigment-Protein Interactions in the Recombinant Water-Soluble Chlorophyll Protein. I. Difference Fluorescence Line-Narrowing. *J. Phys. Chem. B* **2011**, *115*, 4042−4052.

(5) Renger, T.; Marcus, R. A. On the Relation of Protein Dynamics and Exciton Relaxation in Pigment-Protein Complexes: An Estimation of the Spectral Density and a Theory for the Calculation of Optical Spectra. *J. Chem. Phys.* **2002**, *116*, 9997−10019.

(6) Olbrich, C.; Strümpfer, J.; Schulten, K.; Kleinekathöfer, U. Theory and Simulation of the Environmental Effects on FMO Electronic Transitions. *J. Phys. Chem. Lett.* **2011**, *2*, 1771−1776.

(7) Olbrich, C.; Jansen, T. L. C.; Liebers, J.; Aghtar, M.; Strümpfer, J.; Schulten, K.; Knoester, J.; Kleinekathöfer, U. From Atomistic Modeling to Excitation Transfer and Two-Dimensional Spectra of the FMO Light-Harvesting Complex. *J. Phys. Chem. B* **2011**, *115*, 8609−8621.

(8) Shim, S.; Rebentrost, P.; Valleau, S.; Aspuru-Guzik, A. Atomistic Study of the Long-Lived Quantum Coherences in the Fenna-Matthews-Olson Complex. *Biophys. J.* **2012**, *102*, 649−660.

(9) Valleau, S.; Eisfeld, A.; Aspuru-Guzik, A. On the Alternatives for Bath Correlators and Spectral Densities from Mixed Quantum-Classical Simulations. *J. Chem. Phys.* **2012**, *137*, 224103.

(10) May, V.; Kühn, O. *Charge and Energy Transfer Dynamics in Molecular Systems*, 2nd ed.; Wiley-VCH: Weinheim, 2004; pp 128−129.

(11) Mukamel, S. *Principles Nonlinear Optical Spectroscopy*; Oxford University Press: Oxford, 1995; pp 214−234.

(12) Toutounji, M. M.; Small, G. J. The Underdamped Brownian Oscillator Model with Ohmic Dissipation: Applicability to Low-Temperature Optical Spectra. *J. Chem. Phys.* **2002**, *117*, 3848−3855.

(13) Butkus, V.; Valkunas, L.; Abramavicius, D. Molecular Vibrations-Induced Quantum Beats in Two-Dimensional Electronic Spectroscopy. *J. Chem. Phys.* **2012**, *137*, 044513.

(14) Ritschel, G.; Roden, J.; Strunz, W. T.; Eisfeld, A. An Efficient Method to Calculate Excitation Energy Transfer in Light-Harvesting Systems: Application to the Fenna-Matthews-Olson Complex. *New J. Phys.* **2011**, *13*, 113034.

(15) Kolli, A.; O'Reilly, E. J.; Scholes, G. D.; Olaya-Castro, A. The Fundamental Role of Quantized Vibrations in Coherent Light Harvesting by Cryptophyte Algae. *J. Chem. Phys.* **2012**, *137*, 174109.

(16) Reppert, M.; Naibo, V.; Jankowiak, R. Accurate Modeling of Fluorescence Line Narrowing Difference Spectra: Direct Measurement of the Single-Site Fluorescence Spectrum. *J. Chem. Phys.* **2010**, *133*, 014506.

(17) Jankowiak, R.; Reppert, M.; Zazubovich, V.; Pieper, J.; Reinot, T. Site Selective and Single Complex Laser-Based Spectroscopies: A Window on Excited State Electronic Structure, Excitation Energy Transfer, and Electron-Phonon Coupling of Selected Photosynthetic Complexes. *Chem. Rev.* **2011**, *111*, 4546−4598.

(18) Lin, C.; Reppert, M.; Feng, X.; Jankowiak, R., to be submitted for publication, 2013.

(19) Adolphs, J.; Renger, T. How Proteins Trigger Excitation Energy Transfer in the FMO Complex of Green Sulfur Bacteria. *Biophys. J.* **2006**, *91*, 2778−2797.

(20) Renger, T.; Trostmann, I.; Theiss, C.; Madjet, M. E.; Richter, M.; Paulsen, H.; Eichler, H. J.; Knorr, A.; Renger, G. Refinement of a Structural Model of a Pigment-Protein Complex by Accurate Optical Line Shape Theory and Experiments. *J. Phys. Chem. B* **2007**, *111*, 10487−10501.

(21) Raszewski, G.; Renger, T. Light Harvesting in Photosystem II Core Complexes is Limited by the Transfer to the Trap: Can the Core Complex Turn into a Photoprotective Mode? *J. Am. Chem. Soc.* **2008**, *130*, 4431−4446.

(22) Renger, T.; Madjet, M. E.; Knorr, A.; Müh, F. How the Molecular Structure Determines the Flow of Excitation Energy in Plant Light-Harvesting Complex II. *J. Plant Physiol.* **2011**, *168*, 1497−1509.
(23) Pieper, J.; Schödel, R.; Irrgang, K.-D.; Voigt, J.; Renger, G. Electron-Phonon Coupling in Solubilized LHC II Complexes of Green Plants Investigated by Line-Narrwoing and Temperature-Dependent Fluorescence Spectroscopy. *J. Phys. Chem. B* **2001**, *105*, 7115−7124.
(24) Jang, S.; Silbey, R. J. Single Complex Line Shapes of the B850 Band of LH2. *J. Chem. Phys.* **2003**, *118*, 9324−9336.
(25) Jang, S.; Newton, M. D.; Silbey, R. J. Multichromophoric Förster Resonance Energy Transfer from B800 to B850 in the Light Harvesting Complex 2: Evidence for Subtle Energetic Optimization by Purple Bacteria. *J. Phys. Chem. B* **2007**, *111*, 6807−6814.
(26) Jang, S.; Silbey, R. J.; Junz, R.; Hofmann, C.; Köhler, J. Is There Elliptic Distortion in the Light Harvesting Complex 2 of Purple Bactera? *J. Phys. Chem. B* **2011**, *115*, 12947−12953.
(27) Kumar, P.; Jang, S. Emission Lineshapes of the B850 Band of the Light-Harvesting 2 (LH2) Complex in Purple Bacteria: A Second Order Time-Nonlocal Quantum Master Equation Approach. *J. Chem. Phys.* **2013**, *138*, 135101.
(28) Jang, S.; Cao, J.; Silbey, R. J. On the Temperature Dependence of Molecular Line Shapes Due to Linearly Coupled Phonon Bands. *J. Phys. Chem. B* **2002**, *106*, 8313−8317.
(29) Renger, T. Theory of Optical Spectra Involving Charge Transfer States: Dynamic Localization Predicts a Temperature Dependent Optical Band Shift. *Phys. Rev. Lett.* **2004**, *93*, 188101.
(30) Kreisbeck, C.; Kramer, T. Long-Lived Electronic Coherence in Dissipative Exciton Dynamics of Light-Harvesting Complexes. *J. Phys. Chem. Lett.* **2012**, *3*, 2828−2833.
(31) Chen, L.; Zheng, R.; Jing, Y.; Shi, Q. Simulation of the Two-Dimensional Electronic Spectra of the Fenna-Matthews-Olson Complex Using the Hierarchical Equations of Motion Method. *J. Chem. Phys.* **2011**, *134*, 194508.
(32) Hein, B.; Kreisbeck, C.; Kramer, T.; Rodríguez, M. Modeling of Oscillations in Two-Dimensional Echo-Spectra of the Fenna-Matthews-Olson Complex. *New J. Phys.* **2012**, *14*, 023018.
(33) Novoderezhkin, V. I.; Andrizhiyevskaya, B. G.; Dekker, J. P.; van Grondelle, R. Pathways and Timescales of Primary Charge Separation in the Photosystem II Reaction Center as Revealed by a Simultaneous Fit of Time-Resolved Fluorescence and Transient Absorption. *Biophys. J.* **2005**, *89*, 1464−1481.
(34) Engel, G. S.; Calhoun, T. R.; Read, E. L.; Ahn, T.-K.; Mančal, T.; Cheng, Y.-C.; Blankenship, R. E.; Fleming, G. R. Evidence for Wavelike Energy Transfer Through Quantum Coherence in Photosynthetic Systems. *Nature* **2007**, *446*, 782−786.
(35) Panitchayangkoon, G.; Hayes, D.; Fransted, K. A.; Caram, J. R.; Harel, E.; Wen, J.; Blankenship, R. E.; Engel, G. S. Long-Lived Quantum Coherence in Photosynthetic Complexes at Physiological Temperature. *Proc. Natl. Acad. Sci. U. S. A.* **2010**, *107*, 12766−12770.
(36) Renger, T.; Klinger, A.; Steinecker, F.; Schmidt am Busch, M.; Numata, J.; Müh, F. Normal Mode Analysis of the Spectral Density of the Fenna-Matthews-Olson Light-Harvesting Protein: How the Protein Dissipates the Excess Energy of Excitons. *J. Phys. Chem. B* **2012**, *116*, 14565−14580.
(37) Feng, X.; Kell, A.; Pieper, J.; Jankowiak, R. Modeling of the Optical Spectra of the Light-Harvesting CP29 Antenna Complex of Photosystem II − Part II. *J. Phys. Chem. B* **2013**, *117*, 6593−6602.
(38) Renger, G.; Pieper, J.; Theiss, C.; Trostmann, I.; Paulsen, H.; Renger, T.; Eichler, H. J.; Schmitt, F.-J. Water Soluble Chlorophyll Binding Protein of Higher Plants: A Most Suitable Model System for Basic Analyses of Pigment-Pigment and Pigment-Protein Interactions in Chlorophyll Protein Complexes. *J. Plant Physiol.* **2011**, *168*, 1462−1472.
(39) Renger, T.; Madjet, M. E.; Müh, F.; Trostmann, I.; Schmitt, F.-J.; Theiss, C.; Paulsen, H.; Eichler, H. J.; Knorr, A.; Renger, G. Thermally Activated Superradiance and Intersystem Crossing in the Water-Soluble Chlorophyll Binding Protein. *J. Phys. Chem. B* **2009**, *113*, 9948−9957.
(40) Cho, M.; Vaswani, H. M.; Brixner, T.; Stenger, J.; Fleming, G. R. Exciton Analysis in 2D Electronic Spectroscopy. *J. Phys. Chem. B* **2005**, *109*, 10542−10556.
(41) Nalbach, P.; Eckel, J.; Thorwart, M. Quantum Coherent Biomolecular Energy Transfer with Spatially Correlated Fluctuations. *New J. Phys.* **2010**, *12*, 065043.
(42) Mohseni, M.; Rebentrost, P.; Lloyd, S.; Aspuru-Guzik, A. Environment-Assisted Quantum Walks in Photosynthetic Energy Transfer. *J. Chem. Phys.* **2008**, *129*, 174106.
(43) Kreisbeck, C.; Kramer, T.; Rodríguez, M.; Hein, B. High-Performance Solution of Hierarchical Equations of Motion for Studying Energy Transfer in Light-Harvesting Complexes. *J. Chem. Theory Comput.* **2011**, *7*, 2166−2174.
(44) Abramavicius, D.; Voronine, D. V.; Mukamel, S. Unraveling Coherent Dynamics and Energy Dissipation in Photosynthetic Complexes by 2D Spectroscopy. *Biophys. J.* **2008**, *94*, 3613−3619.
(45) Ishizaki, A.; Fleming, G. R. Theoretical Examination of Quantum Coherence in a Photosynthetic System at Physiological Temperature. *Proc. Natl. Acad. Sci. U. S. A.* **2009**, *106*, 17255−17260.